Available online at www.sciencedirect.com
SCIENCE DIRECT
C. R. Mecanique 333 (2005) 87–94
COMPTES RENDUS MECANIQUE
http://france.elsevier.com/direct/CRAS2B/

High-Order Methods for the Numerical Simulation of Vortical and Turbulent Flows

Direct numerical simulation of the interaction of isotropic turbulence with a shock wave using shock-fitting

Jörn Sesterhenn, Jean-François Dohogne, Rainer Friedrich

Fachgebiet Strömungsmechanik, Technische Universität München, Boltzmannstrasse 15, 85748 Garching, Germany

Available online 4 January 2005

Abstract

The interaction of three-dimensional isotropic turbulence with a plane shock at Mach numbers of $M = 2.0$ and $M = 3.0$ is investigated via direct numerical simulation. The numerical scheme is based on a characteristic-type formulation of the Navier–Stokes equations and uses fifth-order upwind schemes in space, a fourth order Runge Kutta scheme in time and a shock-fitting as inlet condition. The isotropic turbulence was generated in a separate computation based on a prescribed energy spectrum. This turbulent flow is considered as frozen, and is convected through the shock with a prescribed average shock speed. An FFT interpolation is used to obtain the upstream values at the instantaneous shock location. Turbulence enhancement is observed, and the evolution of velocity fluctuations as well as turbulence microscales are in good agreement with the behaviour observed using shock-capturing. ***To cite this article: J. Sesterhenn et al., C. R. Mecanique 333 (2005).***

Keywords: Computational fluid mechanics; Characteristic-type formulation; Shock-fitting; Turbulence microscales

1. Introduction

The interaction of turbulence with a shock wave is of great practical importance in many fields of engineering. The knowledge of the physics of this process is crucial for future development of hypersonic aircrafts, supersonic combustion, prediction of sound emission and more. Velocity fluctuations and length scales of the turbulent flow are substantially changed due to the shock.

Kovasznay [1] showed that, to first order, acoustic-, vortical- and entropy-fluctuations are decoupled in turbulent flows. One main feature of shock-turbulence interaction is the strong coupling of these modes.

Several approaches to compute the interaction of turbulence and shock waves exist. Besides linear interaction analysis [2] and rapid distortion theory [3], three different numerical approaches exist: (i) direct numerical simulation (DNS) which implies integration of the Navier–Stokes equations through the shock without model assumptions; (ii) shock-fitting which essentially means neglecting the shock-thickness and applying the Rankine–

E-mail address: Joern.Sesterhenn@lrz.tum.de (J. Sesterhenn).

1631-0721/$ – see front matter
doi:10.1016/j.crme.2004.09.017

Hugoniot relations; and lastly (iii) filtering the equations. This can be achieved by use of a shock-capturing scheme or explicit filtering of the equations. From the viewpoint of the turbulent field, a DNS, a large eddy simulation (LES) or a Reynolds averaged (RANS) computation may be envisaged, all of which give different results [4].

In the present article a DNS of the turbulent flow field in conjunction with a shock-fitting method is employed and compared with other approaches. It is planned to perform full DNS and LES computations as well, in the future, to investigate the differences between these approaches.

2. Governing equations

The numerical code is based on a reformulation of the three-dimensional Navier–Stokes equations which expresses the inviscid part of the equations as a decomposition into acoustic and convective waves, aligned with the numerical grid.

$$
\begin{aligned}
p_\tau &= -\frac{\rho c}{2}\big[[X^+ + X^-] + [Y^+ + Y^-] + [Z^+ + Z^-]\big] + \frac{p}{c_v}[s_\tau + X^s + Y^s + Z^s] \\
u_\tau &= -\frac{\sqrt{g^{11}}}{2}[X^+ - X^-] - Y^u - \frac{g^{21}}{2\sqrt{g^{22}}}[Y^+ - Y^-] - Z^u - \frac{g^{31}}{2\sqrt{g^{33}}}[Z^+ - Z^-] + \frac{\xi^1_{,i}\xi^l_{,j}}{\rho}\frac{\partial \tau_{ij}}{\partial \xi^l} \\
v_\tau &= -X^v - \frac{g^{12}}{2\sqrt{g^{11}}}[X^+ - X^-] - \frac{\sqrt{g^{22}}}{2}[Y^+ - Y^-] - Z^v - \frac{g^{32}}{2\sqrt{g^{33}}}[Z^+ - Z^-] + \frac{\xi^2_{,i}\xi^l_{,j}}{\rho}\frac{\partial \tau_{ij}}{\partial \xi^l} \\
w_\tau &= -X^w - \frac{g^{13}}{2\sqrt{g^{11}}}[X^+ - X^-] - Y^w - \frac{g^{23}}{2\sqrt{g^{22}}}[Y^+ - Y^-] - \frac{\sqrt{g^{33}}}{2}[Z^+ - Z^-] + \frac{\xi^3_{,i}\xi^l_{,j}}{\rho}\frac{\partial \tau_{ij}}{\partial \xi^l} \\
s_\tau &= -X^s - Y^s - Z^s + \frac{1}{\rho T}\left(\phi - \xi^k_{,i}\frac{\partial}{\partial \xi^k}\left(\lambda \xi^l_{,i}\frac{\partial T}{\partial \xi^l}\right)\right)
\end{aligned}
\tag{1}
$$

with the abbreviations:

$$
\begin{aligned}
X^\pm &:= \big(u \pm \sqrt{g^{11}}c\big)\left[\frac{p_\xi}{\rho c} \pm \frac{u|_\xi}{\sqrt{g^{11}}}\right]; \qquad X^s := u s_\xi \\
Y^\pm &:= \big(v \pm \sqrt{g^{22}}c\big)\left[\frac{p_\eta}{\rho c} \pm \frac{v|_\eta}{\sqrt{g^{22}}}\right]; \qquad Y^s := v s_\eta \\
Z^\pm &:= \big(w \pm \sqrt{g^{33}}c\big)\left[\frac{p_\zeta}{\rho c} \pm \frac{w|_\zeta}{\sqrt{g^{33}}}\right]; \qquad Z^s := w s_\zeta \\
X^v &:= u\left(v|_\xi - \frac{g^{12}}{g^{11}}u|_\xi\right); \qquad X^w := u\left(w|_\xi - \frac{g^{13}}{g^{11}}u|_\xi\right) \\
Y^u &:= v\left(u|_\eta - \frac{g^{21}}{g^{22}}v|_\eta\right); \qquad Y^w := v\left(w|_\eta - \frac{g^{23}}{g^{22}}v|_\eta\right) \\
Z^u &:= w\left(u|_\zeta - \frac{g^{31}}{g^{33}}w|_\zeta\right); \qquad Z^v := w\left(v|_\zeta - \frac{g^{32}}{g^{33}}w|_\zeta\right)
\end{aligned}
$$

A complete description of this method is given by Sesterhenn [5]. (p, u, v, w, s) signify pressure, contravariant velocities and entropy. $X^\pm$, $Y^\pm$ and $Z^\pm$ represent acoustic waves travelling normally to constant coordinate surfaces ξ^1, ξ^2 and ξ^3, respectively. X^v, X^w, Y^u, etc. describe the transport of vorticity along the appropriate directions. X^s, Y^s, Z^s model the convective transport of entropy waves. Thus, the decomposition may be viewed as a normal wave decomposition in computational space. The derivatives are approximated using a compact upwind scheme of fifth order [6].

To this Euler part of the Navier–Stokes equations the viscous and heat-conduction terms are added. Φ is the viscous dissipation rate $\tau_{ij}\frac{\partial u_i}{\partial x_j}$. Dissipative terms are discretized using a sixth order central scheme similar to [7]. g_{lm} is the metric tensor, defined by $g_{lm} = \xi^l_{,i}\xi^m_{,i}$.

3. Boundary conditions

The computational domain consists in the subsonic flow downstream of the shock which coincides with the west boundary of the domain. The east boundary is prescribed as a nonreflecting outlet, north, south front and back are treated periodically. The physical domain is time dependent and the grid distorts with the movement of the shock boundary. In this work, we consider the case of a decaying isotropic turbulent flow, which is periodic in all three space directions as it moves through a shock. Since the flow is supersonic it is not aware of the shock and may be computed in a separate DNS.

Thus, we have a supersonic inlet boundary condition beyond the shock boundary. This condition consists in imposing the values of the time derivatives of pressure, velocity components and entropy at the boundary according to the isotropic field. Together with one characteristic entering the shock from the high pressure side, those values determine the time derivatives at the downstream side. They are calculated from the corresponding upstream values, using the Rankine–Hugoniot conditions [8]. With this method, the shock is considered as a discontinuity. This is acceptable as long as the length scales of the flow $\eta \approx (\nu^3/\epsilon)^{1/4}$ up- and downstream of the shock are much bigger than the shock thickness δ_u. As long as this condition is satisfied, the resolution of the grid is determined by the smallest turbulent length scales of the flow only and not by the shock thickness.

Given an isotropic turbulent flow field, the turbulence will decay since a forcing is absent. On the other hand a statistically stationary turbulent flow behind a mesh is known to be approximately homogeneous in planes perpendicular to the flow direction. To avoid computing a spatially decaying, but locally stationary turbulent flow, we compute an isotropic flow and consider an instantaneous field at a certain time and simulate the nonvanishing mean flow of our model by translating the field with a constant speed s.

In order to impose the supersonic inlet boundary condition on the moving shock, the upstream values of the time derivatives

$$\frac{\mathrm{d}}{\mathrm{d}t} = \frac{\partial}{\partial t} + U_i\frac{\partial}{\partial x_i}$$

of pressure, velocity and entropy at any grid point of the shock are needed. $U_i = \{u_s - s, v_s, w_s\}$ are the Cartesian components of the local shock velocity in a reference frame moving with the average shock-speed, identified with s.

In this case, the values of the time derivatives of pressure, velocity and entropy just before the shock are given by convective terms only:

$$\frac{\mathrm{d}}{\mathrm{d}t} = (u_s - s)\frac{\partial}{\partial x} + v_s\frac{\partial}{\partial y} + w_s\frac{\partial}{\partial z} \tag{2}$$

The three-dimensional isotropic turbulent flow used to calculate the flow variables upstream of the shock consists in a periodic arrangement of a 'turbulent box'. Initially it has a kinetic energy spectrum of the form

$$E(k) \propto u_0^2/k_0(k/k_0)^4\exp(-2k^2/k_0^2)$$

where k_0 is the peak wavenumber and u_0 the initial rms-value of the velocity fluctuation in any direction. The same spectrum was used in [9] and [10] by Lee et al. as well as in [11] and [12] by Hannappel and Friedrich in their DNS of the interaction of isotropic turbulence with a shock. The choice of this spectrum is justified by its good representation of low-Reynolds-number turbulence.

Subsequently, the flow is allowed to evolve until the artificial initial field has relaxed to a physically reasonable flow field. This is checked by the skewness being $S \approx -0.4$.

Once we have the turbulent upstream flow at our disposal, the problem is that we only know the pressures, velocities and entropies at a discrete set of points of the 'turbulent box'. As we convect this field through the shock, the points representing the shock surface are to be found between grid points. So we need interpolations to obtain the physical values at the desired points, that is on those situated on the shock, on the upstream side of it. Thus, we use an interpolation based on a Fourier transform and a phase shift corresponding to the local shock velocity of the physical values of the 'turbulent box'. This is relatively cheap since the shock curvature remains small and a one-dimensional interpolation in the x-direction suffices. At the same time the method is accurate. However, we would like to add that other interpolation methods would work as well and are in fact necessary if the incoming flow is not periodic.

A drawback of the present method is the fact that all quantities are convected with the shock speed whereas in reality different wave speeds are present on the upstream side. A simple, but costly remedy is to perform a simultaneous DNS for the upstream side. To prevent the decay of the turbulence a forcing might be added. This is planned for future investigations.

4. Results

For the two simulations presented in this article we have used the parameter values upstream of the shock given in Table 1.

The isotropic turbulence was generated, as described above with 96^3 grid points. M_1 is the upstream value of the Mach Number, $M_t = u_o/\bar{c}$ the turbulent Mach Number, η_1 the upstream value of the Kolmogorov length scale and $Re_\lambda = \bar{\rho} u_0 \lambda/\bar{\mu}$ a Reynolds number based on the Taylor microscale, λ, relative to a component of the velocity fluctuation. The bar denotes an ensemble average. In order to be allowed to apply shock-fitting, we have to be sure that the shock-thickness (δ_u) is much smaller than the length scales of the flow upstream and downstream. So we calculated the shock thicknesses in both cases and compared them to the corresponding Kolmogorov length scales directly downstream of the shock, η_2, which we obtained, a posteriori, from the DNS (Table 2).

To estimate the velocity-gradient thickness we may use $\delta_u \approx \frac{\nu}{c}\frac{6.89}{M-1}$ [13] which is valid for weak shocks. As we can see in both cases, η_2 is clearly greater (alas not much greater) than the shock thickness. Thus, shock-fitting is applicable and in any case better than a shock capturing since the shock thickness would artificially increase in that case.

The Kolmogorov length scale immediately downstream of the shock is the smallest of all turbulent length scales of the problem, so that the shock thickness is much smaller than almost all turbulent length scales.

To arrive at an expression for the behaviour of η/δ_u, we estimate further the Kolmogorov scale of the isotropic turbulence by using $\epsilon \approx 15\nu u_{\mathrm{rms}}^2/\lambda^2$[14]. Rearranging η/δ_u we get

Table 1
Parameter values upstream of the shock

Case	M_1	M_t	Re_λ	k_0	η_1
I	2.0	0.0352	3.39	45 000	1.0E–5
II	3.0	0.0352	3.39	45 000	1.0E–5

Table 2
Kolmogorov length scales downstream of the shock

Case	δ_u	η_2	η_2/δ_u
I	1E–6	5.11E–6	≈ 5
II	7E–7	4.32E–6	≈ 6

$$\frac{\eta}{\delta_u} \approx \frac{(\nu^3/\epsilon)^{1/4}}{(\nu/c)(6.89/(M_1-1))} \approx \frac{1}{8}\frac{M_1-1}{M_t}\sqrt{Re_\lambda} \tag{3}$$

Thus for larger Re_λ the ratio gets more favourable, since the shock thickness reduces more rapidly when reducing ν than η does.

The downstream side of the shock was computed with 96^3 grid points as well, but the grid was stretched to cluster points in the vicinity of the shock. To compute the average values plotted in the figures of this work, we first calculated average values on planes parallel to the shock and situated at different distances x away from the shock. Those planes contained 96^2 points in each case. Then we averaged those values in time, the number of instantaneous values used for this purpose was 153 for case I, and 143 for case II.

4.1. Evolution of velocity fluctuations

Fig. 1 shows the evolution of the diagonal components of the Reynolds stress tensor, $R_{ij} = \widetilde{u_i'' u_j''}$, in both our simulations. u_i'' is the fluctuation of u_i with respect to its average $\widetilde{u_i} = \overline{\rho u_i}/\overline{\rho}$, introduced by Favre in [15]. Note that the graphs in this article show dimensionless quantities as they are scaled using the values u_0 and k_0 of the simulation that is referred to. The off-diagonal components (not represented) stay closely to zero over the entire flow since turbulence is isotropic upstream and then axisymmetric downstream of the shock.

As a consequence of axisymmetry, we found the profiles of both transverse velocity fluctuations, $\widetilde{u_2''^2}/u_0^2$ and $\widetilde{u_3''^2}/u_0^2$, to coincide. Thus, we plotted only one of them in each case. Directly after the shock, the streamwise fluctuation is reduced whereas the transverse fluctuations are amplified. Then the velocity fluctuations evolve rapidly just downstream of the shock, within a distance of the same order of magnitude as k_0^{-1}. This phenomenon is due to the evanescent acoustic waves that are produced by the shock-turbulence interaction, as predicted by Ribner through linear analysis in [2]. The rapid evolution consists in a decay of the transverse velocity fluctuations and an increase of the streamwise fluctuation. After that, all the velocity fluctuations decay monotonically due to viscous

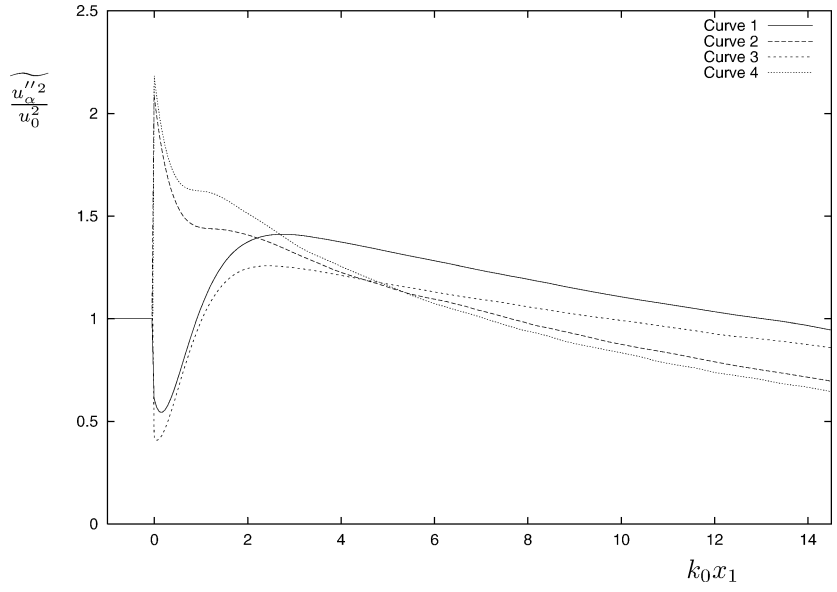

Fig. 1. Evolution of the normal components of the Reynolds stress: Curve 1 stands for the streamwise component ($\widetilde{u_1''^2}/u_0^2$) at $M_1 = 2.0$, Curve 2 for a transverse component ($\widetilde{u_2''^2}/u_0^2$) at $M_1 = 2.0$, Curve 3 for $\widetilde{u_1''^2}/u_0^2$ at $M_1 = 3.0$, Curve 4 for $\widetilde{u_2''^2}/u_0^2$ at $M_1 = 3.0$.

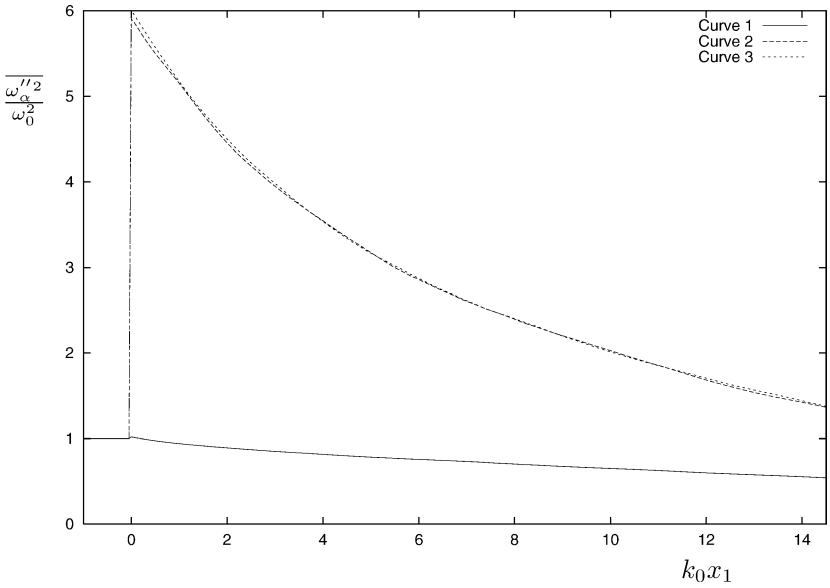

Fig. 2. Evolution of the vorticity fluctuations for $M_1 = 2.0$ (Case I). Curve 1 stands for the streamwise fluctuation, Curves 2 and 3 for the transverse fluctuations. For a given simulation, the corresponding reference vorticity ω_0 is the upstream RMS-value of the vorticity fluctuation in any direction.

dissipation. This effect is dominant far from the shock, and the return to isotropy is negligible comparing to it. The same behaviour of the turbulent velocity components was observed by Lee et al. [10], using shock-capturing, and the comparison of Fig. 1 with Fig. 3(a) of [10] confirms the good agreement of both DNS, even if they were performed with different values of Re_λ. The quoted results as well as measurements show a high peak of $\widetilde{u_1''^2}/u_0^2$ within the shock zone, which is not present in our computation. This peak is mainly due to the oscillation of the shock relative to a fixed point in space where the measurements are taken [9]. In our case the measurements (numerical or experimental) are taken in a location which is fixed with respect to the shock and always located downstream of it.

4.2. Vorticity fluctuations

In quasi-incompressible fluctuating flows like those considered in this paper and in [10], vorticity fluctuations are clearly the main contributor to the dissipation rate of the turbulent kinetic energy. Fig. 2 shows the evolution of the components of vorticity fluctuations. We can see that, directly downstream of the shock, transverse components are amplified and the streamwise component is hardly affected. The amplification ratio of approximately 6 for the transverse components observed in Fig. 2 (as well as in Fig. 5(a) in [10]) agrees with the predictions of the linear analysis for $M_1 = 2.0$ (see Fig. 5(b) from [10] for the latter). Amplification ratios found for other values of M_1 in this work, as well as in [10] were also consistent with linear analysis.

4.3. Microscales

Fig. 3 shows the evolution of the Taylor microscales, λ_i, and the transverse density microscale λ_ρ obtained in the present DNS. These length scales are defined as

$$\lambda_i = \frac{(\overline{u_i'^2})^{1/2}}{(\overline{(\partial u_i'/\partial x_i)^2})^{1/2}} \quad \text{(no summation convention is used for } i\text{)} \quad \text{and} \quad \lambda_\rho = \frac{(\overline{\rho'^2})^{1/2}}{(\overline{(\partial \rho'/\partial x_2)^2})^{1/2}}$$

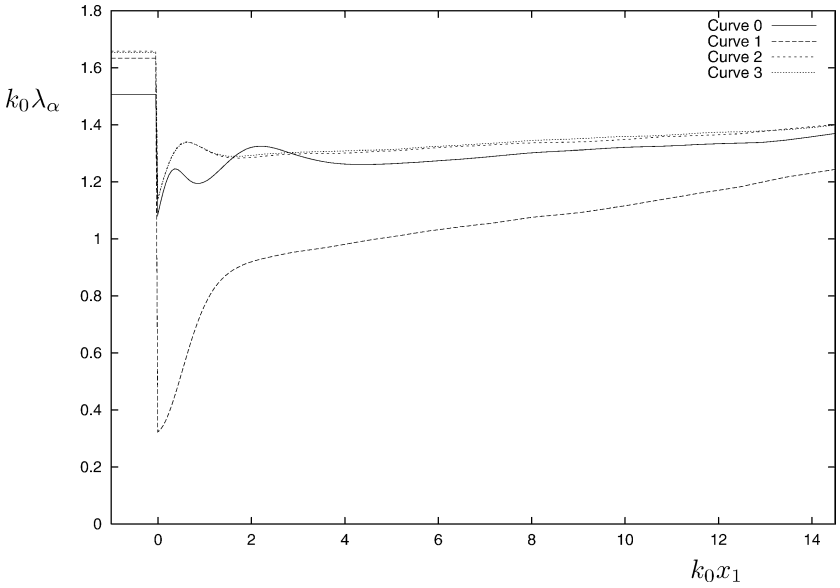

Fig. 3. Evolution of microscales by our DNS for $M_1 = 2.0$ (Case I). Curve 0 stands for λ_ρ, Curves $i = 1, 2, 3$ for λ_i.

The evolution of those microscales obtained by the DNS of Lee et al. are shown in Fig. 9(a) of [10]. Both DNS reveal a decrease of the four microscales considered here; moreover they both show the decrease of the streamwise Taylor microscale to be greater than that of the transverse Taylor microscales. Those features are also explained by a linear analysis performed in [10] by Lee et al.

5. Conclusions and recommendations

Shock-turbulence interaction was studied using a high-order upwind scheme together with a shock fitting method. Agreement is observed between the results of the present DNS and those of other simulations as well as the conclusions of linear analysis. Nevertheless, more simulations need to be performed to further validate the results and to assess the use of these methods within the scope of shock-turbulence interaction. Moreover, this work considered the interaction of a shock with a 'frozen' periodic isotropic turbulence convected through the shock. Thus, acoustical waves, moving with different speeds are not represented properly. To avoid this, future DNS should calculate both upstream and downstream flow simultaneously (but still on two different grids). Doing so, the temporal evolution of the upstream turbulence would be taken into account, which is desirable for computing acoustic fluctuations accurately. In order to keep the mean energy of the upstream flow constant, a forcing term should be added to the Navier–Stokes equations. Shock-fitting bases on the hypothesis that the typical length scales of the simulated flow have to be much greater than the shock thickness, δ_u. The present work shows that $\eta \approx 5\delta_u$ seems to be sufficient for the successful use of shock-fitting by simulations of shock-turbulence interaction. The effect of the ratio of turbulent length scales to shock thickness on the results of the DNS should be investigated more accurately to find where practical limits are situated. Lee et al. predict a saturation of the amplification rate of turbulent kinetic energy for M_1 beyond 3.0 (see [10]). As this prediction is only based on linear analysis, it should be verified through DNS for several values of M_1 beyond 3.0. This should be easier to realize with shock-fitting than with shock-capturing. The reason for that is clear, shock-capturing needs a finer resolution as the shock thickness decreases with growing shock strength. On the contrary, shock-fitting considers the shock as a discontinuity

and is therefore particularly appropriate for DNS of strong shocks. This last point illustrates the biggest advantage of using shock-fitting while studying the interaction of turbulence with a shock.

Considering LES, the finest resolved scales are always (by construction) of the same size as the apparent shock thickness. What this means for the accuracy of the shock-turbulence interaction is not clear yet. The favourable comparison of the present computations with a shock-capturing scheme indicates that the Reynolds-stresses will be computed accurately away from the shock. The computation of noise emitted from the shock might be affected more strongly by this coincidence of the lengthscales than the other methods.

References

[1] L.S.G. Kovasznay, Turbulence in supersonic flow, J. Aeronaut. Sci. 20 (1953) 657–674.
[2] H.S. Ribner, Convection of a pattern of vorticity through a shock wave, Technical Report TR 1164, NACA, 1953.
[3] L. Jacquin, E. Blin, P. Geffroy, Turbulence amplification by a shock wave and rapid distortion theory, Phys. Fluid. A 5 (1992) 2539–2550.
[4] Y. Andreopoulos, J.H. Agui, G. Briassulis, Shock wave-turbulence interactions, Annu. Rev. Fluid Mech. 32 (2000) 309–345.
[5] J. Sesterhenn, A characteristic-type formulation of the Navier–Stokes equations for high order upwind schemes, Comput. Fluids 30 (1) (2001) 37–67.
[6] N.A. Adams, K. Shariff, A high-resolution hybrid compact-ENO scheme for shock-turbulence interaction problems, J. Comput. Phys. 127 (1996) 27–51.
[7] S.K. Lele, Compact finite difference schemes with spectral-like resolution, J. Comput. Phys. 103 (1992) 16–42.
[8] D. Fabre, L. Jacquin, J. Sesterhenn, Linear interaction of a cylindrical entropy spot with a shock, Phys. Fluids 13 (8) (2001) 2403–2422.
[9] S. Lee, P. Moin, S.K. Lele, Interaction of isotropic turbulence with a shock wave, Technical Report TF-52, Department of Mechanical Engineering, Stanford University, 1992.
[10] S. Lee, S.K. Lele, P. Moin, Interaction of isotropic turbulence with shock waves: effect of shock strength, J. Fluid Mech. 340 (1997) 225–247.
[11] R. Hannappel, Direkte numerische Simulation der Wechselwirkung eines Verdichtungsstoßes mit isotroper Turbulenz, PhD thesis, Technische Universität München, 1995.
[12] R. Hannappel, R. Friedrich, Direct numerical simulation of a Mach 2 shock interacting with isotropic turbulence, Appl. Sci. Res. 54 (1995) 205–221.
[13] E. Becker, Gasdynamik, Teubner, Stuttgart, 1966.
[14] H. Tennekes, J.L. Lumley, A First Course in Turbulence, MIT Press, 1972.
[15] A. Favre, Equations des gaz turbulents compressibles ii, J. Mécanique 4 (1965) 391–421.